Acta Crystallographica Section D
Biological Crystallography
ISSN 0907-4449

Structure determination of an anti-HIV-1 Fab 447-52D–peptide complex from an epitaxially twinned data set

Amandeep K. Dhillon,[a] Robyn L. Stanfield,[b,c] Miroslaw K. Gorny,[d] Constance Williams,[d] Susan Zolla-Pazner[d] and Ian A. Wilson[b,c]*

[a]Department of Immunology, The Scripps Research Institute, 10550 North Torrey Pines Road, La Jolla, California 92037, USA, [b]Department of Molecular Biology, The Scripps Research Institute, 10550 North Torrey Pines Road, La Jolla, California 92037, USA, [c]The Skaggs Institute for Chemical Biology, The Scripps Research Institute, 10550 North Torrey Pines Road, La Jolla, California 92037, USA, and [d]New York VA Medical Center and New York University School of Medicine, New York, New York 10010, USA

Correspondence e-mail: wilson@scripps.edu

Received 11 February 2008
Accepted 9 May 2008

PDB Reference: anti-HIV-1 Fab 447-52D–peptide complex, 3c2a, r3c2asf.

Although antibodies against the third variable loop (V3) of the HIV-1 viral envelope glycoprotein are among the first neutralizing antibodies to be detected in infected individuals, they are normally restricted in their specificity. X-ray crystallographic studies of V3-specific antibodies have contributed to a more thorough understanding of recognition of this epitope and of conserved features in the V3 loop that could potentially aid in the design of a multi-component vaccine. The human antibody 447-52D exhibits relatively broad neutralization of primary viral isolates compared with other V3-loop antibodies. A crystal structure of Fab 447-52D in complex with a V3 peptide (UG1033) was determined at 2.1 Å resolution. The structure was determined using an epitaxially twinned data set and in-house programs to detect and remove overlapping reflections. Although the processed data have lower than desired completeness and slightly higher than normal R values for the resolution, good-quality electron-density maps were obtained that enabled structure determination. The structure revealed an extended CDR H3 loop that forms a β-sheet with the peptide, with the predominant contacts being main-chain hydrogen bonds. The V3 peptide and Fab show high structural homology with the previously reported structures of other Fab 447-52D complexes, reinforcing the idea that the V3 loop may adopt a small set of conserved structures, particularly around the crown of the β-hairpin.

1. Introduction

The human immunodeficiency virus type 1 (HIV-1) envelope is a highly glycosylated trimer of heterodimers, composed of gp120, which mediates binding to the cell-surface CD4 receptor and chemokine co-receptors, and gp41, a transmembrane protein that is involved in membrane fusion. Despite its exposure on the viral surface, the HIV-1 envelope spike, which is the target of neutralizing antibodies, has evolved many diverse mechanisms to escape the humoral immune response. Extensive glycosylation of the exposed envelope protein, which gives rise to an immunologically silent 'glycan shield', and exposure of regions of gp120 that are highly variable in sequence, termed the V1–V5 hypervariable loops, are among the major mechanisms that contribute to the ability of HIV-1 to evade the antibody response during infection (Burton *et al.*, 2005; Pantophlet & Burton, 2006; Wei *et al.*, 2003; Wyatt *et al.*, 1998). The glycan shield results in a general dampening of the immune response, whereas the immunodominant variable loops tend to elicit neutralizing antibodies that exhibit strain-specific neutralization.

Table 1
Comparison of the six different data-processing and initial test refinements of the epitaxially twinned data.

Data set no.	1 Lattice 1	2 Lattice 2	3 Lattice 1 + 2	4 Lattice 1†	5 Lattice 2†	6 Lattice 1 + 2†
No. of spots‡	2346478	2350364	4696842	1810397	1814960	3625357
No. of overlapping spots deleted by in-house program	0	0	0	536081	535405	1071485
No. of observations§	206766	215665	427782	153463	159567	310899
No. of observations rejected by *SCALEPACK*	26884	29981	89699	15236	15350	49923
No. of unique reflections¶	68033	68897	69984	56663	57482	60586
Completeness (%)	96.9	97.4	98.9	80.6	81.3	85.7
Redundancy	3.0	3.1	6.1	2.7	2.8	5.1
$\langle I/\sigma(I)\rangle$	23.6	24.1	34.4	19.5	19.7	27.1
$R_{\rm merge}$	6.7 (32.9)	6.7 (34.5)	8.3 (39.4)	6.8 (38.7)	6.9 (38.8)	8.4 (44.5)
$R_{\rm rigid}$††	38.1	37.6	37.7	36.7	36.6	36.4
$R_{\rm cryst}/R_{\rm free}$	30.9/34.4	30.4/33.7	30.3/34.2	29.7/33.2	29.4/33.9	29.1/32.9

† The last three columns are with overlaps manually deleted, whereas the first three columns are with no manual deletion of overlapping spots. ‡ Spots are defined as the two-dimensional diffraction peak from a single image frame. In most cases, these are partial reflections. § Observations are the integrated intensity formed by the profile-fitted summation of the partial spots. ¶ Reflections are the average of multiply measured and symmetry-related observations. †† $R_{\rm rigid}$ is the $R_{\rm cryst}$ value from the initial rigid-body refinement with resolution limits of 15–4 Å.

The third hypervariable (V3) loop of gp120 was initially known as the principal neutralizing determinant of HIV-1 owing to its ability to readily elicit anti-HIV-1 antibodies (Gao *et al.*, 2005; Goudsmit *et al.*, 1988; Javaherian *et al.*, 1989, 1990; Rusche *et al.*, 1988). The anti-V3 antibodies induced early in infection and after limited exposure to immunogens are relatively type-specific; however, anti-V3 antibodies that display broader reactivity have been reported (Binley *et al.*, 2004; Gorny *et al.*, 2002, 2006; Krachmarov *et al.*, 2005; Pantophlet *et al.*, 2007; Richman *et al.*, 2003). The neutralization activity of anti-V3 antibodies may be affected by the propensity of the V3 region to undergo sequence changes that alter neutralizing-antibody epitopes and give rise to escape mutants during the course of infection (Hartley *et al.*, 2005; Richman *et al.*, 2003), epitope masking by the V1/V2 domain (Hartley *et al.*, 2005; Pantophlet & Burton, 2006; Pinter *et al.*, 2004) and/or the presence of glycans (Back *et al.*, 1994; Koch *et al.*, 2003; McCaffrey *et al.*, 2004).

However, human V3-specific monoclonal antibodies (mAbs) have been described that exhibit neutralization of multiple primary HIV-1 isolates, suggesting that this region may indeed be a worthwhile target in a multi-component HIV-1 vaccine. The antibody 447-52D, which was originally isolated from an HIV-1-infected individual (Gorny *et al.*, 1992, 1993), is one of several anti-V3 monoclonal antibodies (Gorny *et al.*, 2004, 2006) that exhibit significant neutralizing breadth (Binley *et al.*, 2004). Immunochemical studies mapped the core epitope to a GP*x*R motif in the crown of the V3 loop (Keller *et al.*, 1993). Although this motif is prevalent within subtype B isolates, the dominant crown motif of non-clade-B isolates is GPGQ (http://www.hiv.lanl.gov/content/hiv-db). In one analysis, Fab 447-52D neutralized 50% of 32 clade-B viruses (Binley *et al.*, 2004); in a second study, 92% of 38 primary isolates containing the GPGR crown motif could be neutralized (Zolla-Pazner *et al.*, 2004). The V3-specific mAb 2219, which was also derived from an HIV-1-infected individual, similarly exhibits neutralization of a relatively large proportion of HIV-1 isolates (Gorny *et al.*, 2002, 2004). More recently, human mAb F425-B4e8 has been reported to exhibit cross-neutralizing activity comparable to those of Fab 447-52D and Fab 2219 (Pantophlet *et al.*, 2007).

In addition to being a potential target for a neutralizing epitope in an HIV-1 vaccine, the V3 loop plays an important role in virus infectivity. The sequence of the V3 loop can influence cell tropism (Hoffman & Doms, 1999) and this loop is thought to interact with the chemokine co-receptors CCR5 or CXCR4 during infection (Basmaciogullari *et al.*, 2002; Rizzuto & Sodroski, 2000; Rizzuto *et al.*, 1998). The V3 region is composed of approximately 35 residues and contains a conserved disulfide bridge at the base of the loop. A recent crystal structure of an HIV-1 gp120 core containing an intact V3 loop reveals that this region contains three structurally distinct domains: a conserved base, a crown or tip region (apex) and a flexible stem that links the base and crown (Huang *et al.*, 2005). Antibody-binding studies performed in the presence of soluble CD4 suggest that the V3 loop may become more accessible upon CD4 binding (Mbah *et al.*, 2001). Such an extended structure could help to explain the immunodominance of the V3 loop. Cryo-electron tomography studies performed with SIV virions suggest two possible models for the location of the V3 loop within the context of the trimeric envelope. In the first, the V3 loop is solvent-exposed and positioned away from the trimer interface along the outer side of gp120 (Zhu *et al.*, 2006). Alternatively, the V3 region may be packed into the trimer interface and become exposed upon CD4-envelope ligation owing to structural rearrangement of the trimer (Zanetti *et al.*, 2006).

To gain a better understanding of the conformation of the V3 loop and of the basis for neutralization by V3 mAbs, structural studies of anti-V3 mAbs in complex with V3 peptides have been undertaken. To date, X-ray crystallographic structures of four murine anti-V3 Fabs (50.1, 58.2, 59.1, 83.1) have been determined for the Fabs in complex with V3 peptides corresponding to the HIV-1 isolate MN (Ghiara *et al.*, 1994, 1997; Rini *et al.*, 1993; Stanfield *et al.*, 1993, 1999, 2003). The crystal structure of human Fab 447-52D has also been determined in complex with an MN peptide (Stanfield *et al.*, 2004) and, more recently, crystal structures of Fab 2219 in

Table 2
Processing and final refinement statistics for data set 6.

Values in parentheses are for the last shell.

Data collection	
Space group	$P2_1$
Unit-cell parameters (Å, °)	a = 70.5, b = 75.9, c = 114.1, β = 101.5
Resolution (Å)	50–2.1 (2.15–2.10)
No. of observations	310899 (13751)
No. of unique reflections	60586 (3035)
Completeness (%)	85.7 (86.0)
Redundancy	5.1 (4.5)
$\langle I/\sigma(I)\rangle$	27.1 (4.0)
$R_{\rm merge}$	8.4 (44.5)
Refinement statistics	
$R_{\rm cryst}$	24.1 (29.9)
$R_{\rm free}$	29.8 (37.5)
No. of waters	188
R.m.s.d. from ideal geometry	
Bond lengths (Å)	0.017
Angles (°)	1.6
B values† (Å^2)	
Fab 1	
V_L	29.4
C_L	31.1
V_H	34.1
C_H1	31.3
Peptide	57.8
Fab 2	
V_L	53.7
C_L	52.2
V_H	49.8
C_H1	39.9
Peptide	82.8
Waters	34.6
Overall	40.8
Ramachandran plot	
Most favored (%)	88.5
Additionally allowed (%)	11.0
Generously allowed (%)	0.1
Disallowed (%)	0.4

† B values are the sum of TLS and residual B factors.

complex with three different V3 peptides, corresponding to isolates UG1033, MN and UR29, have been reported (Stanfield, Gorny *et al.*, 2006).

The MN V3 peptide adopts a similar conformation in complex with the murine Fabs 50.1, 59.1 and 83.1, whereas a different V3-crown structure is observed in the Fab 58.2 complex. In the former, residues upstream of the crown form an extended β-sheet, with a type I or II β-turn around the GPGR crown motif. The V3 peptide in the Fab 58.2 complex adopts a different conformation at the crown that contains two consecutive turns. The V3 peptides in the Fab 447-52D and Fab 2219 crystal structures show structural homology to these murine Fab complexes, adopting β-hairpin structures, although the relative orientation of the N- and C-terminal strands in the Fab 2219 peptides differs owing to a differing torsion angle of a single residue within the N-terminal strand. These V3 structures are also comparable to the conformation observed in the V3-containing core gp120 structures (Huang *et al.*, 2005, 2007; Stanfield & Wilson, 2005). Finally, NMR studies of the Fv fragment of 447-52D in complex with V3 peptides corresponding to isolates MN and IIIb show that the peptides in both of these complexes form β-hairpin structures and exhibit the same N-terminal conformation (Rosen *et al.*, 2005; Sharon *et al.*, 2003).

Here, we report the processing strategy for an epitaxially twinned data set (Table 1) and the details of the resulting 2.1 Å structure of the UG1033 V3 peptide bound to Fab 447-52D. We also discuss insights gained from a comparative analysis of this new structure with those previously reported for other V3-peptide complexes of Fab 447-52D.

2. Experimental

2.1. Fab production and purification

IgG 447-52D (IgG3, λ) was produced and purified as previously reported (Gorny *et al.*, 1989, 1991). Briefly, pooled peripheral blood cells from two HIV-1-infected patients were transformed and fused to a human/mouse hetero-myeloma cell line (SHM-D33). The Mab 447-52D heterohybridoma was selected based on its ability to bind a peptide corresponding to a portion of the V3 sequence of the HIV-1 isolate MN (YNKRKRIGIGPGRAFYTTKNIIG) and then repeatedly cloned until monoclonality was achieved. Fab fragments were prepared by IgG 447-52D cleavage with 4% papain in 10 m*M* L-cysteine for 4 h. Fab 447-52D was purified on Protein A, Superdex 200 (10/30 column; 0.2 *M* sodium acetate pH 5.5) and Mono S columns (10/10 column; buffer *A* = 50 m*M* sodium acetate pH 4.5; buffer *B* = 50 m*M* sodium acetate, 1 *M* sodium chloride pH 4.5).

2.2. Crystallization

A 23-mer V3 peptide, UG1033 (NNTRKSIHLGPGRAFYATGDIIG), was used for cocrystallization. Fab 447-52D (20 mg ml^{-1}) and UG1033 peptide were mixed in a 1:5 molar ratio and crystals were grown using the standard sitting-drop vapor-diffusion method. Thin intergrown crystal plates which could not be readily separated were grown from 1.4 *M* ammonium sulfate, 0.1 *M* cacodylate pH 6.5 and did not diffract beyond 2.5 Å. However, screening of these conditions with Hampton Additive Screen 1 revealed larger single-crystal plates with $CuCl_2$ as an additive. Crystals that visually appeared to be single were grown using a final reservoir solution of 1.58 *M* ammonium sulfate, 0.1 *M* Tris pH 7.88, 1 m*M* $CuCl_2$. Crystals were cryopreserved by brief immersion into a solution consisting of the reservoir solution augmented with 25% glycerol. Data were collected to 2.1 Å resolution on SSRL beamline 11-1 with a 0.25° step size and a crystal-to-detector distance of 250 mm on an ADSC Q315 detector and reduced in space group $P2_1$ with unit-cell parameters a = 70.5, b = 75.9, c = 114.1 Å, β = 101.5°. The Matthews coefficient was 3.0 Å^3 Da^{-1} (Matthews, 1985), corresponding to 59% solvent content. Data were indexed, integrated and scaled with *HKL*-2000 (Otwinowski & Minor, 1997) to 2.1 Å resolution (Table 2). Multiple lattices were detected in all crystals that were screened. Twinned data sets were resolved using *DENZO*/*SCALEPACK* (Otwinowski & Minor, 1997) and in-house programs, as described below in §3.

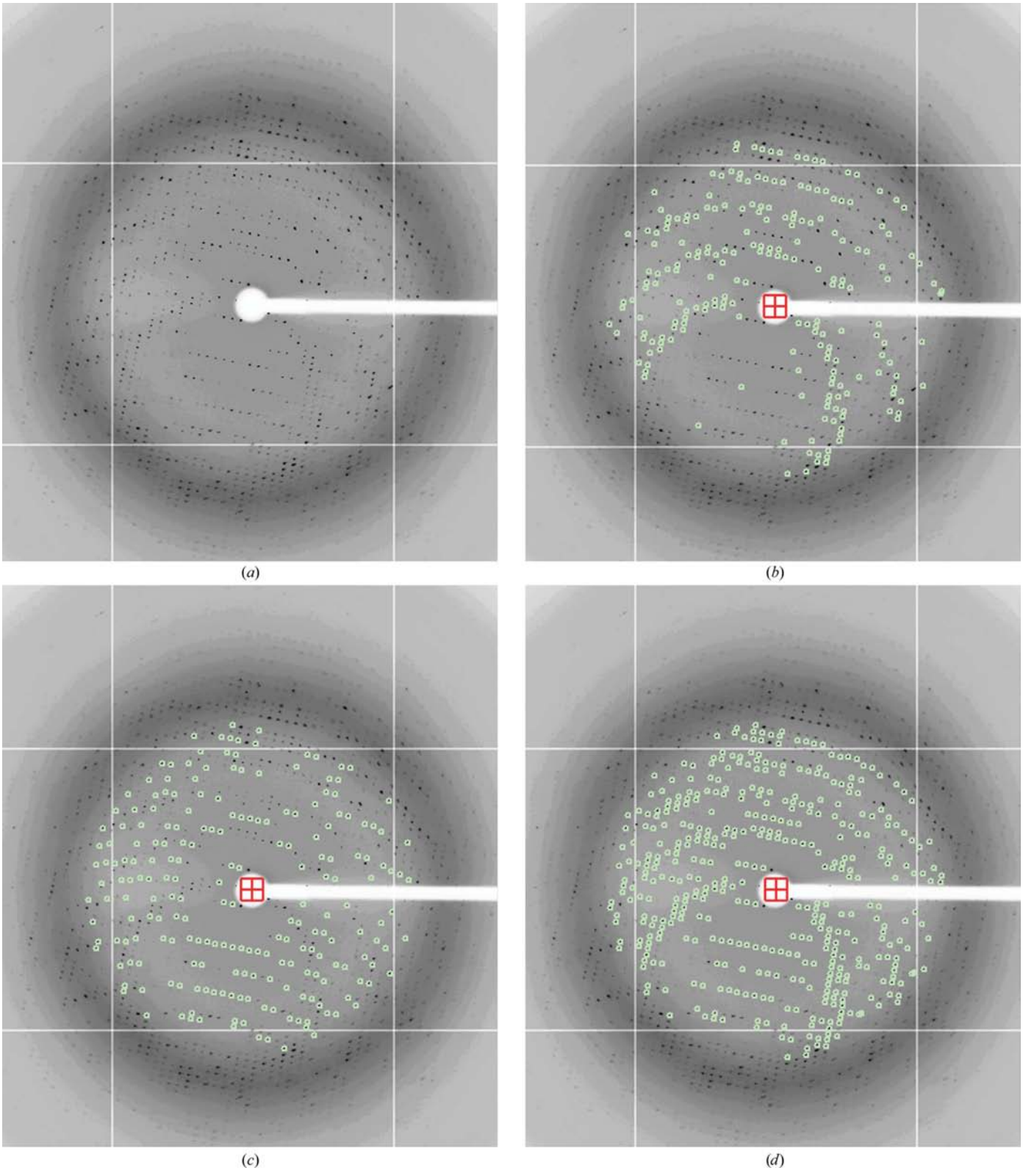

Figure 1
Raw data from the epitaxially twinned data set. The frames are displayed with the *XDISPLAYF* (Otwinowski & Minor, 1997) software, and the images have been cropped to show only the strongly diffracting spots. (*a*) The first diffraction image (crystal to detector distance = 250 cm, oscillation angle = 0.25°). (*b*) Spots (diffraction maxima) corresponding to the first lattice are shown in green, after separation of the spot file into two files for the two different lattices, as described in §3. (*c*) Spots (green) corresponding to the second lattice. (*d*) The same image with all spots (green) from both lattices selected for auto-indexing by *XDISPLAYF*.

2.3. Structural determination and refinement

The structure was determined by molecular replacement using the refined structure of Fab 447-52D (PDB code 1q1j) as a search model. Two Fab–peptide complexes were present in the asymmetric unit and were related by an NCS twofold around x (or z). Alternating cycles of model building and positional refinement were carried out using *TOM*/*FRODO* (Jones, 1982) and *CNS* (Brünger *et al.*, 1998). Tight NCS restraints were used early in refinement and then gradually released. Final rounds of refinement were carried out using *REFMAC* (Collaborative Computational Project, Number 4, 1994) with eight TLS groups corresponding to C_L, V_L, C_H1 and V_H + peptide for each Fab complex. B values for all protein domains and solvent molecules are reported in Table 2. An R_{free} test set of 5% of the reflections was maintained throughout refinement. Electron-density maps used for rebuilding included σ_A-weighted $2F_o - F_c$ and $F_o - F_c$ maps. Hydrogen bonds and van der Waals contacts were evaluated with *HBPLUS* (McDonald & Thornton, 1994) and *CONTACSYM* (Sheriff *et al.*, 1987). Buried molecular-surface areas were calculated using the program *MS* (Connolly, 1993) with a 1.4 Å probe radius.

3. Results and discussion

3.1. Lattice separation in the epitaxially twinned crystals

Although the crystals grown in the presence of $CuCl_2$ diffracted strongly, they contained two separate lattices of approximately equivalent intensity with the same unit-cell parameters, as if two crystals in different orientations had intergrown (Fig. 1). Multiple crystals were tested, but none were obtained with a single lattice. Attempts to obtain strongly diffracting crystals under alternative growth conditions also failed. As a result, data from the epitaxially twinned crystals were collected and processed with *DENZO*/*SCALEPACK* (Otwinowski & Minor, 1997) and in-house programs, as detailed below, to include data from both lattices. While published descriptions of computer programs for treating epitaxially twinned data processed with *XDS* (Lietzke *et al.*, 1996) and *XENGEN* (Schulze-Gahmen *et al.*, 1993) are available, we were unable to find any similar programs that worked with *DENZO*/*SCALEPACK*. Since this work was carried out, a web-based server has been developed in another laboratory that works with *DENZO*/*SCALEPACK* using a similar scheme to that which we describe here (http://ultr23.vub.ac.be/untangle).

Firstly, a standard *DENZO*/*XDISP* peak search was used to find spots on the first diffraction image. The term 'spots' will be used throughout to define two-dimensional diffraction peaks from a single image that result, in most cases, from partial reflections. The spots representing both lattices were used in the initial *DENZO* autoindexing. The autoindexing routine then calculates a unit cell and orientation matrix for one of the two lattices and using this information 'spots' from 'lattice 1' only were integrated. An in-house program was then used to compare the x, y centroid position of each integrated spot from lattice 1 with the spot positions found by *XDISP*. The *XDISP* spots were then separated into two files, one containing the spots within two pixels (1 pixel = 0.1024 mm) of integrated spots from lattice 1 and a second file containing the remaining spots, which predominantly belong to lattice 2 (Fig. 1). Each of these *XDISP* spot files was used as input to the autoindexing routine in *DENZO*, resulting in a unit cell and orientation matrix for each lattice. All frames were then integrated twice, once with each orientation matrix, resulting in files containing integrated spots from each of the two lattices. The two lattices are related by an approximate twofold rotation around the c axis of the crystal.

To deal with the problem of overlapping spots that arise from both lattices, another program was written to read in the files containing the integrated spots for each lattice on a frame-by-frame basis and then delete spots whose predicted centroid positions (in pixel units) are within two pixels (1 pixel = 0.1024 mm) of each other. The partial spots were then summed and profile-fitted to create the integrated intensities (observations) and scaled using *SCALEPACK* (to obtain unique reflections) for each of the individual lattices and also for the merged lattices (lattice 1 + 2) with and without overlapping-spot deletion. We generated six data sets using these criteria (see Table 1) in order to evaluate the best method for treating these data. Two to three rounds of initial model refinement with *CNS* were then carried out with each data set to determine which would yield the best quality model, as judged by R values and stereochemistry. Structures could be readily refined with all six data sets (see §2) with electron-density maps of similar quality. The R_{cryst} and R_{free} values are also very similar (Table 1). The final structure reported here was determined at 2.1 Å from the sixth data set in Table 1, which was chosen because it had the lowest R_{cryst}/R_{free} values of the six data sets. The final statistics listed in Table 2 are for the sixth data set, but with model rebuilding and complete refinement in addition to the preliminary refinements reported for the initial tests of the six data sets in Table 1.

3.2. Structure of Fab 447-52D

Fab 447-52D was crystallized with a 23-mer V3 peptide designated UG1033 (NNTRKSIHLGPGRAFYATGDIIG). Processing and refinement statistics for the 2.1 Å structure are reported in Table 2. The crystallographic asymmetric unit contains two Fab complexes related by a noncrystallographic (NCS) twofold axis around x (or z). Slightly higher B values and weaker electron density were observed in the second Fab complex, indicating a higher degree of flexibility for this complex. The C^{α} r.m.s. deviations for the equivalent variable light-chain (V_L) and heavy-chain (V_H) regions are 0.31 and 0.22 Å, respectively, and 0.43 Å for the V3 peptide. Because the two structures are so similar, only the first of the two molecules is discussed here unless noted otherwise. The Fab chains are numbered according to the Kabat and Wu convention (Kabat *et al.*, 1987) and the peptide is numbered according to the HIV-1 HxBc2 numbering convention (Ratner *et al.*, 1987). The heavy and light chains are designated chains

H and L for Fab 1 and chains I and M for Fab 2, respectively, and the peptides are designated chains P and Q for Fabs 1 and 2, respectively. The elbow angles of the two Fabs are 212° and 207°, which are consistent with rather large elbow angles frequently observed for other Fabs with λ light chains (Stanfield, Zemla *et al.*, 2006). Only three residues in the two complexes fall in the disallowed region of the Ramachandran plot. Asn^{L51} and Asn^{M51} are in a highly conserved γ-turn that is found in almost all Fabs (Stanfield *et al.*, 1999) and Asp^{M151} is in a loop which also has well ordered density. One residue, Ser^{H134}, lies within the generously allowed region of the Ramachandran plot and is within in a poorly ordered region of C_H1 that tends to be disordered in most Fabs. Although $CuCl_2$ was part of the crystallization solution, no density was found that could be assigned to copper or chloride ions.

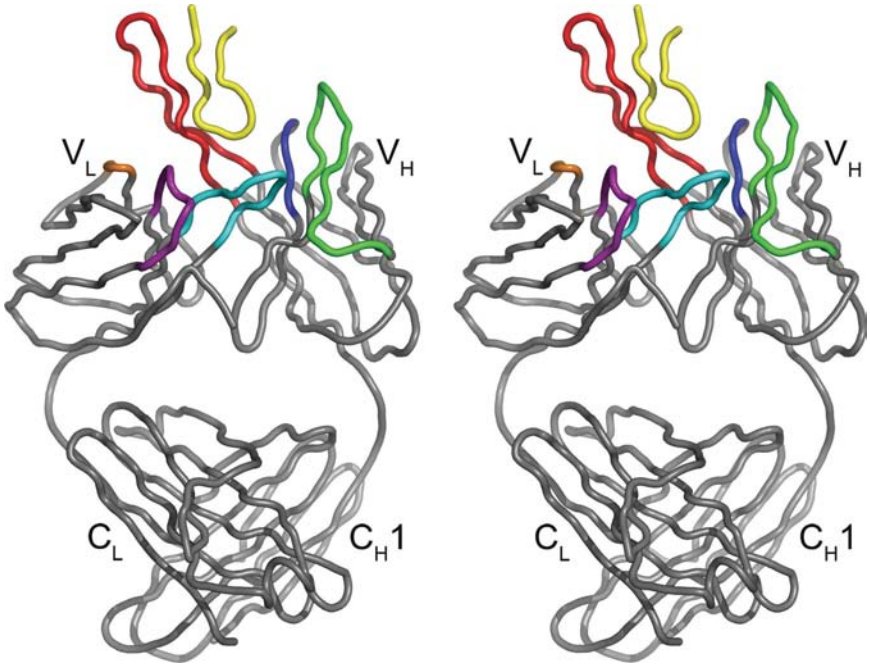

Figure 2
Stereoview of the Fab 447-52D–UG1033 peptide complex. The Fab is colored gray, with the light chain oriented to the left and the heavy chain oriented to the right. Complementarity-determining regions (CDRs) L1, L2 and L3 are colored purple, orange and cyan, respectively. CDRs H1, H2 and H3 are colored blue, green and red, respectively. The UG1033 V3 peptide is colored yellow. This and subsequent figures were generated with *PyMOL* (DeLano, 2002).

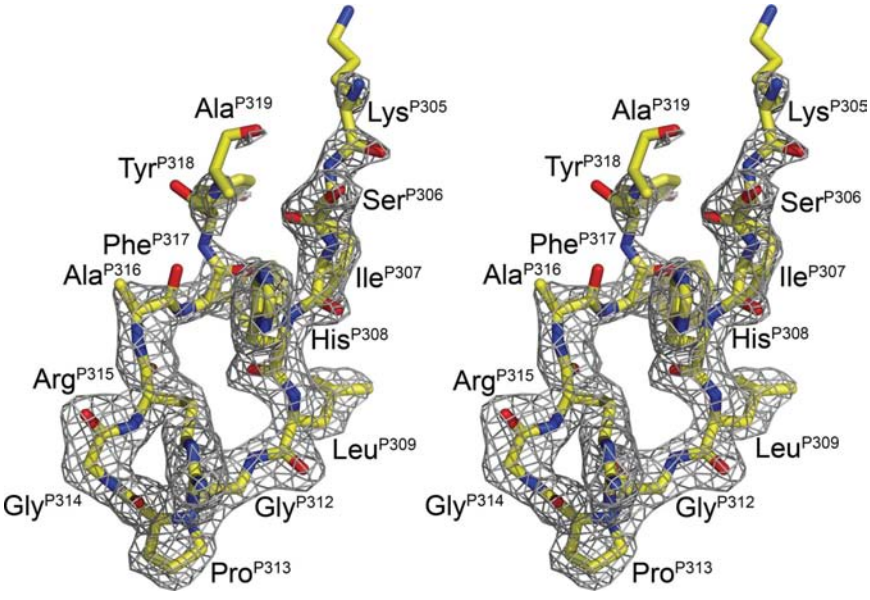

Figure 3
Stereoview of electron density of the UG1033 peptide bound to Fab 447-52D. The $2F_o - F_c$ electron density (gray) for the UG1033 V3 peptide (yellow) after refinement is contoured at 1.0σ.

The majority of contacts between the extended CDR H3 loop.

An overview of the Fab 447-52D structure is illustrated in Fig. 2. As expected based on length and sequence, the light-chain CDR1 and CDR2 belong to canonical classes λL1-1 and L2-2 and the heavy-chain CDR1 and CD2 to classes 1 and 4, respectively. As reported previously, the light-chain CDR3 of Fab 447-52D contains a three-residue insertion (L95a–L95c) that makes it longer than other CDR L3 loops classified to date (Stanfield *et al.*, 2004). The 20-residue heavy-chain CDR3 (H3) forms an extended structure, approximately 32 Å from base to tip, which projects outwards from the molecule. The extended structure is stabilized by a hydrogen-bonding network between the N- and C-terminal regions of

3.3. Structure of the UG1033 V3 peptide

The majority of clade A and C isolates contain the V3-crown sequence GPGQ. However, the clade A UG1033 sequence corresponds to the dominant crown motif, GPGR, typically found in clade B. Although the UG1033 peptide is 23 residues in length, strong interpretable electron density was only present for ten residues (Fig. 3). Weaker electron density was present for an additional three residues (Phe^{P317}, Tyr^{P318} and Ala^{P319}), which are also included in the final model. The remaining C-terminal residues could not be built into the final model owing to very weak electron density, which is likely to be a consequence of the conformational flexibility of this region of the peptide, as frequently observed in other V3-loop complexes with Fabs (Ghiara *et al.*, 1994, 1997; Rini *et al.*, 1993; Stanfield *et al.*, 1993, 1999, 2003, 2004; Stanfield, Gorny *et al.*, 2006).

The V3 peptide binds alongside the extended CDR H3 (Fig. 2), forming a three-stranded mixed β-sheet with CDR H3 (Fig. 4*a*). The majority of contacts between

Table 3
Backbone torsion angles for the UG1033 peptide structures complexed with Fab 447-52D and Fab 2219 and the equivalent V3 loop from a gp120 structure.

	φ (°), UG1033 V3 in			ψ (°), UG1033 V3 in		
Residue	Fab 447-52D	Fab 2219†	gp120 V3‡	Fab 447-52D	Fab 2219†	gp120 V3‡
305	n/a	−78	−124	135	−30	−12
306	−140	−70	−147	125	138	146
307	−103	−109	−118	138	120	160
308	−125	−85	−129	114	106	121
309	−113	−73	−84	94	−39	140
312	−170	−165	−158	171	−175	131
313	−71	−60	−59	138	126	99
314	78	71	100	2	12	8
315	−91	−139	−172	134	144	149
316	−69	−158	−13	190	154	167
317	−21	−109	−133	−61	157	153
318	−87	54	60	158	38	65
319	−156	−88	−150	n/a	170	−2

† Torsion angles were calculated from the structure with PDB code 2b1a. ‡ Torsion angles are those reported by Stanfield, Gorny *et al.* (2006) from analysis of the structure with PDB code 2b4c (Huang *et al.*, 2005).

the Fab and peptide are main-chain hydrogen bonds between the N-terminal half of the peptide and the C-terminal portion of the CDR H3 (Fig. 4*b*), although with fewer regular hydrogen bonds to the fourth strand. Five main-chain hydrogen bonds are formed between the following Fab and V3-peptide residues in the two independent complexes: Asp^{H100f} N—Lys^{P305} O (3.2/3.1 Å), Asp^{H100f} O—Ile^{P307} N (2.8/2.6 Å), Tyr^{H100h} N—Ile^{P307} O (2.8/2.8 Å), Tyr^{H100h} O—Leu^{P309} N (2.8/2.8 Å), Tyr^{H100j} N—Leu^{P309} O (3.0/3.0 Å). A sixth hydrogen bond is made between the side chains of His^{P308} $N^{\delta1}$ and Tyr^{H100j} OH (2.5/2.6 Å). The peptide is also anchored into the Fab-binding site by a salt bridge between the side chains of Arg^{P315} NH1 and Asp^{H95} $O^{\delta2}$ (2.5/2.5 Å; Fig. 4*c*) and Arg^{P315} also forms π–cation interactions with Trp^{H33} and Tyr^{H100j}. The guanidinium moiety of Arg^{P315} is sandwiched between the indole ring of Trp^{H33} and the phenyl ring of Tyr^{H100j}, with distances of approximately 3.7 and 3.5 Å from the N^{ϵ} atom of Arg^{P315} to the center of the tyrosine and tryptophan rings, respectively. Pro^{P313} is cradled between the indoles of Trp^{L91} and Trp^{L96} in the antibody-combining site (Fig. 4*c*). The conserved V3-crown motif, GPGR, forms a type II β-turn (φ_{i+1} = −71°, ψ_{i+1} = 138° for Pro^{P313}, φ_{i+2} = 78°, ψ_{i+2} = 2° for Gly^{P314}), as previously observed in the Fab 447-52D in complex with an MN V3 peptide (Stanfield *et al.*, 2004).

110 and 141 van der Waals interactions are made in the two Fab–peptide complexes, respectively. The buried molecular-surface areas of the Fab and peptide are 553/587 and 522/487 Å^2 for the two Fab–peptide complexes. The buried surface area of the Fab is largely formed by aromatic tyrosine and tryptophan residues (69%/65%), followed by acidic (19%/20%), basic (6.4%/6.2%), polar (2.4%/4.1%) and small and/or hydrophobic residues (3.3%/4.9%).

3.4. Comparison with the Fab 447-52D–MN V3-peptide complex

Only minor differences are observed between the structure of the Fab 447-52D complex reported above and the Fab 447-52D–MN V3 peptide complex previously reported by our group (Stanfield *et al.*, 2004) based on comparisons calculated using the first molecule of the asymmetric unit of each crystal structure. When the most highly ordered residues in the peptides are superimposed (Lys^{P305}–Ala^{P316}), the r.m.s. deviation (r.m.s.d.) of the C^{α} backbone for the different V3 peptides is 0.45 Å, with the largest deviation (1.0 Å) being at Ala^{P316} (Fig. 5). The UG1033 V3-peptide structure extends an additional three residues beyond Ala^{P316}, although the density

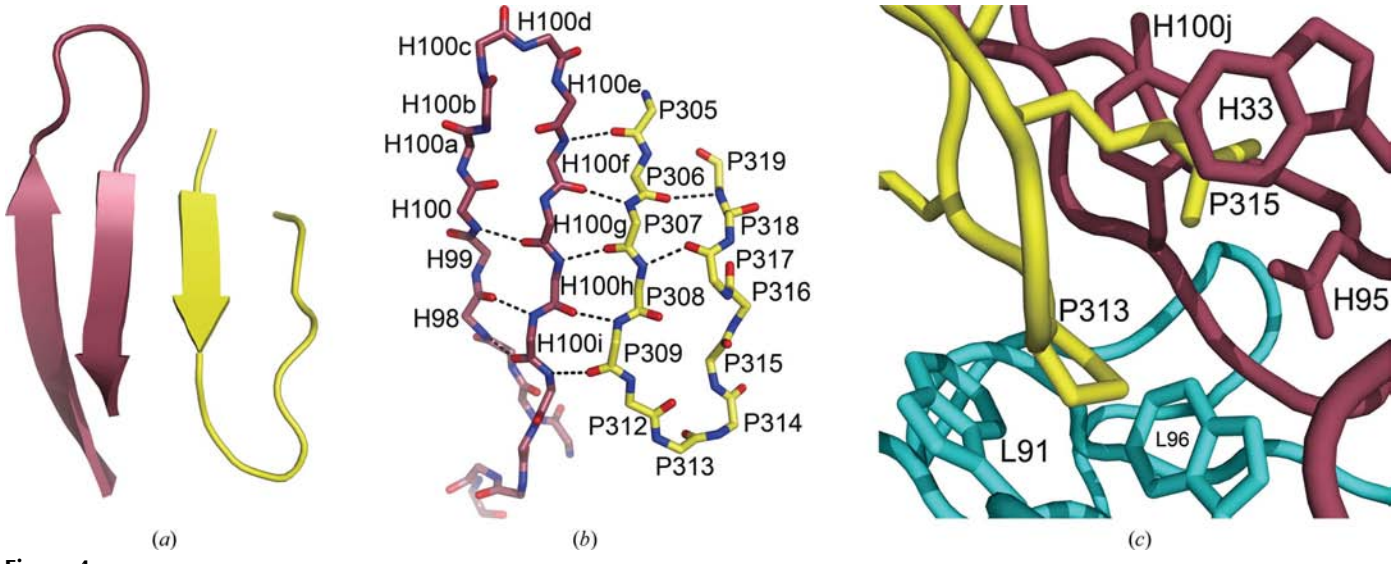

Figure 4
Binding-site interactions between the UG1033 V3 peptide and Fab 447-52D. The Fab CDR H3 is shown in violet and the UG1033 peptide in yellow. (*a*) The mixed three-strand β-sheet formed by CDR H3 and the V3 peptide is shown. (*b*) The main-chain hydrogen-bond interactions in the three-strand β-sheet are represented by black dotted lines. (*c*) Side-chain interactions between the UG1033 peptide and the Fab light chain (cyan) and heavy chain (violet).

for the extra three residues is weak. In the UG1033 V3-peptide structure, Tyr^{P318} contacts a symmetry-related Lys^{L156} in the second molecule in the asymmetric unit, but not in the first molecule. This contact is not made in the MN V3-peptide complex owing to a slight difference in the packing of the molecules. It is not clear whether this contact has helped to stabilize these residues or whether the stronger peptide density is a function of the better diffraction of the UG1033 V3-peptide complex crystals. The GPGR crown motif also adopts a type II β-turn in each of the two structures. The two different Fab 447-52D structures also do not differ significantly, with C$^{\alpha}$ backbone r.m.s.d. values of 0.24 Å for the V_L domain and 0.34 Å for the V_H domain. Notably, inclusion of an additional three residues in the C-terminal portion of the UG1033 peptide also does not increase the peptide-binding interactions with Fab 447-52D.

The UG1033 V3-peptide sequence differs from the MN peptide at two positions. An arginine is present at position P306 and an isoleucine at position P309 in the MN peptide, whereas serine and leucine are found in these positions, respectively, in the UG1033 peptide. However, as expected, these differences in sequence do not affect the main-chain hydrogen bonds that the peptide forms with Fab 447-52D CDR H3. Although P317–P319 at the C-terminus of the UG1033 peptide do not interact with the Fab, they contact the N-terminal strand of the V3 peptide through main-chain hydrogen bonds to form a more regular β-hairpin-type structure. An evaluation of hydrogen-bond contacts detects additional hydrogen bonds in each peptide between Phe^{P317} O and His^{P308} N (2.8/2.6 Å) and a second hydrogen bond in the second peptide between Ala^{Q319} N and Ser^{Q306} O (2.7 Å). The distance between Ala^{P319} N and Ser^{P306} O increases slightly in the first peptide to 3.1 Å, although the density at the C-terminus is weaker.

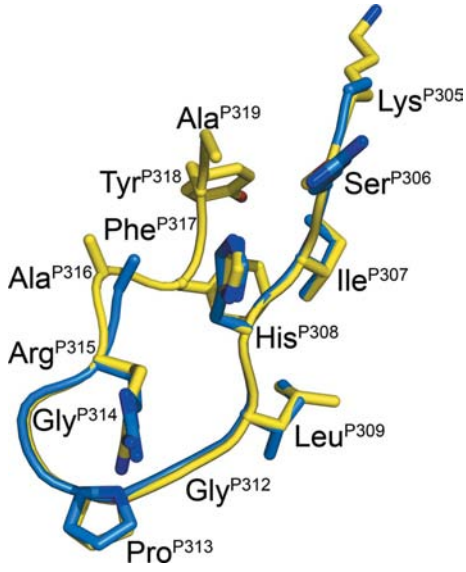

Figure 5
Comparison of the UG1033 and MN peptides bound to Fab 447-52D. A superposition of the C$^{\alpha}$ backbones of the UG1033 V3 peptide bound to Fab 447-52D and the MN V3-peptide structure previously solved in complex with Fab 447-52D is shown. The UG1033 peptide is shown in yellow and the MN peptide in blue. The UG1033-peptide residues are labeled.

3.5. Comparison with Fab 2219–UG1033 and gp120 V3 core structures

The UG1033 peptide structure has also been determined in complex with the V3-specific Fab 2219 (Stanfield, Gorny *et al.*, 2006). As observed here, the GPGR motif also forms a type II β-turn in the Fab 2219 structure, with a C$^{\alpha}$ r.m.s.d. of 0.21 Å to the Fab 447-52D structure (Gly^{P312}–Arg^{P315}). However, a difference in one of the dihedral angles (ψ) of Leu^{P309} results in a change in the orientation of the peptide backbone (Table 3). Hence, the carbonyl O atoms of the N-terminal residues preceding Leu^{P309} are rotated by about 180° in the Fab 2219 complex with respect to the conformation seen in the Fab 447-52D complex (Fig. 6). Despite this difference, the N- and C-terminal strands of the hairpin independently show close structural homology with the UG1033 peptide in the Fab 447-52D structure, with C$^{\alpha}$ backbone r.m.s.d. values of 0.60 Å (Lys^{P305}—Gly^{P312}) and 0.86 Å (Ala^{P316}—Ala^{P319}).

When bound to Fab 2219, the majority of contacts are made through side chains of residues in the N-terminal strand of the UG1033 peptide, although two side-chain contacts from C-terminal residues are also observed. Despite making contact with the Fab 2219, N-terminal residues Thr^{P303}–Ser^{P306} are still solvent-exposed. It is likely that Fab 2219 is able to tolerate diversity in side chains at these positions because of the solvent-accessible nature of these residues. In contrast, the use of main-chain hydrogen-bond contacts allows Fab 447-52D to tolerate diversity within the N-terminal region of the V3. In both structures, Arg^{P315} makes side-chain contacts with the Fab and forms salt bridges to Asn^{L31} in Fab 2219 and to Asp^{H95} in Fab 447-52D. However, the UG1033 V3 crown is also largely accessible in the Fab 2219 complex, whereas it is less accessible and oriented into the antibody-binding pocket in the Fab 447-52D complex reported here.

The structure of the UG1033 V3 peptide in the Fab 447-52D complex also reveals structural homology to the V3 region of gp120-containing V3 crystal structures (Fig. 6). The C$^{\alpha}$ backbone r.m.s.d. values of the UG1033 peptide with the corresponding V3 loop in the reported gp120 V3 structure (Huang *et al.*, 2005) are 0.56 and 0.85 Å for the N-terminal (Lys^{P305}–Gly^{P312}) and C-terminal (Ala^{P316}–Ala^{P319}) strands respectively, and 0.59 Å for the GPGR crown motif. A gp120-containing V3 structure in complex with a tyrosine-sulfated antibody has recently been reported (Huang *et al.*, 2007). The GPGR crown of the V3 loop in this structure exhibits even greater structural homology with the crown of the UG1033 V3 peptide, with a C$^{\alpha}$ backbone r.m.s.d. value of only 0.16 Å.

3.6. Comparison with NMR structures

The structures of MN and IIIB V3 peptides in complex with 447-52D Fv have also been determined by NMR methods. Solution (Sharon *et al.*, 2003) and solid-state (Sharpe *et al.*, 2004) NMR studies of MN V3 peptides (residues 303–325 and 305–322 of the MN V3 loop, respectively) in complex with 447-

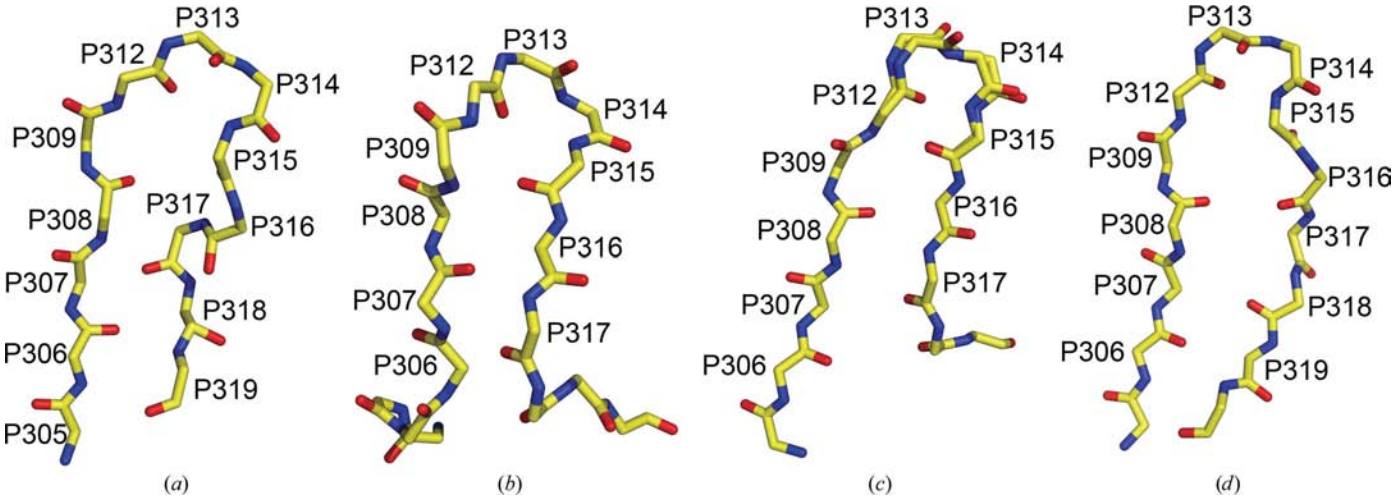

Figure 6
Comparison of V3 crystal structures. The C^{α}-backbone structures are shown in a similar orientations for (*a*) the UG1033 V3 peptide bound to Fab 447-52D (*b*) the UG1033 V3 peptide bound to Fab 2219 (PDB code 2b1a) and the V3 loops from two gp120 core complexes: (*c*) PDB code 2b4c and (*d*) PDB code 2qad. Two conformations were observed for the V3 crown in the core gp120 V3 structure with PDB code 2b4c and both of these conformations are shown in (*c*).

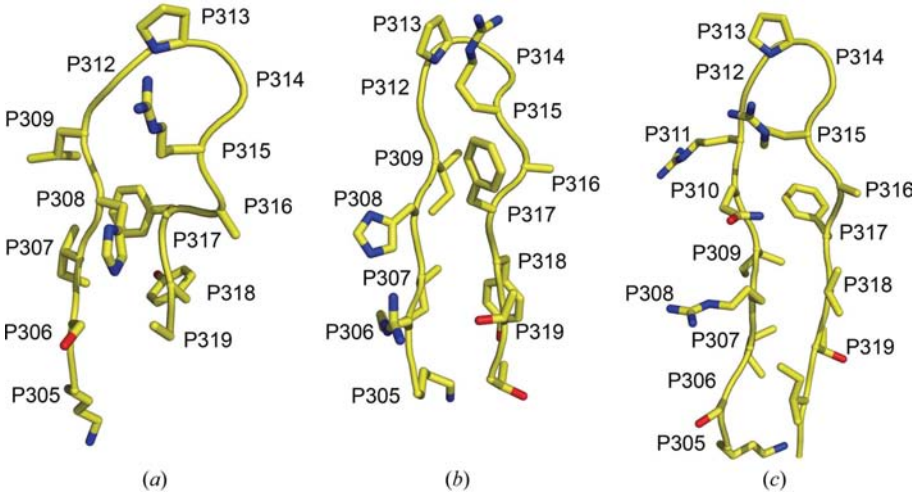

Figure 7
Comparison of the crystal structure of the UG1033 peptide bound to Fab 447-52D with the NMR structures of the MN and IIIB peptides bound to 447-52D Fv. The C^{α}-backbone structures are shown in a similar orientation for (*a*) the UG1033 V3 peptide from the crystal structure and (*b*) MN (PDB code 1n1z) and (*c*) IIIB (PDB code 1u6u) from NMR structures. The N-terminus of each peptide is oriented to the left.

52D Fv show an overall similarity to the structure reported here (Fig. 7). In the NMR studies, the MN peptide forms a β-hairpin stabilized by intrapeptide hydrogen-bond interactions (Gly^{312} O—Gly^{314} N, Arg^{315} O—Thr^{319} N, Thr^{319} O—Arg^{315} N, His^{308} O—Phe^{317} N and Phe^{317} O—His^{308} N) with an inverse γ-turn at the crown. The extended C-terminal portion of the β-hairpin is not observed here, which is likely to be the consequence of flexibility of the C-terminal residues in the UG1033 peptide. However, the overall shape of the peptides is similar (Fig. 7), with a C^{α} r.m.s.d. of 1.7 Å for Lys^{P305}–Ala^{P319}. In the MN–447-52D Fv solution NMR structure, strong interactions between the Fv and peptide are reported for N-terminal peptide residues Lys^{P305}–Arg^{P315} and weaker interactions are reported for the C-terminal Ala^{P316}–Thr^{P320}. Although the same C-terminal interactions are not observed here, the N-terminal residues of the UG1033 peptide still dominate binding to Fab 447-52D. Moreover, in the solid-state NMR structure of the MN V3–447-52D Fv complex, the C-terminal interactions could not be observed. The side chains of Gly^{P312}, Pro^{P313} and Arg^{P315} are also reported to interact with aromatic rings of the Fv in the NMR structures, which is in agreement with our observation that Pro^{P313} is flanked by the indoles of Trp^{L91} and Trp^{L96} and that Arg^{P315} makes π–cation interactions with Tyr^{H100j} and Trp^{H33}.

The NMR structure of a IIIB V3 peptide (residues 303–322) in complex with 447-52D Fv has also been reported (Rosen *et al.*, 2005). The V3 loop of HIV-1_{IIIB} contains a two-residue insertion (QR) before the GPGR crown sequence. In the IIIB V3–Fv structure the peptide forms a β-hairpin, although the QR insertion creates a kink before the β-turn at the crown. Despite the two-residue insertion, the resulting structure is very similar to the UG1033 crystal structure and the MN NMR structure (Fig. 7) discussed above, with the N-terminal residues dominating binding to 447-52D. The similarity of the overall peptide conformation is evident when the UG1033 N-terminal strand (Lys^{P305}–Leu^{P309}), β-turn (Gly^{P312}–Arg^{P315}) and C-terminal strand (Ala^{P316}–Ala^{P319}) are superimposed with the corresponding IIIB peptide residues, giving C^{α} backbone r.m.s.d. values of 0.64, 0.30 and 1.82 Å, respectively. Based on a 2D-homonuclear TOSCY spectrum, Rosen and coworkers also conclude that IIIB residues Ile^{P309} and Gly^{P312} are likely to interact with aromatic tyrosine side

chains of the Fv and Pro^{P313} and Gly^{P314} are likely to interact with tryptophan residues. In the UG1033 structure, Leu^{P309} is positioned near Tyr^{H100i} and Tyr^{L32}, and Gly^{P312}, Pro^{P313} and Gly^{P314} are close to Trp^{L91}, Trp^{L96} and Trp^{H33}. These aromatic contacts are not identical to those proposed in the IIIB–447-52D Fv NMR structure. However, as previously suggested (Rosen *et al.*, 2005), the QR insertion in the IIIB peptide may alter the positioning of the peptide in the 447-52D binding site.

4. Conclusions

The structure of the UG1033 peptide in complex with Fab 447-52D has been determined from an epitaxially twinned data set where the individual lattices were separated and overlapping reflections were removed. The final R_{cryst} and R_{free} values of the model are higher than expected at this resolution, which is likely to be the consequence of some residual overlapping spots (diffraction maxima) that were not removed by the procedure. However, given the quality and resolution of the electron-density maps, the Fab–peptide complex can still be determined with confidence. Moreover, this structure shows very high structural homology to the crystal structure of the MN V3 peptide in complex with Fab 447-52D previously reported by our group (Ghiara *et al.*, 1994, 1997; Rini *et al.*, 1993; Stanfield *et al.*, 1993, 1999, 2003, 2004; Stanfield & Wilson, 2005) and to the NMR structure (Sharon *et al.*, 2003), further validating the final model built from the epitaxially twinned data set.

The structure of the Fab 447-52D complex reported here confirms our previous conclusion that the breadth of this neutralizing antibody is attributable to the use of main-chain hydrogen bonds to contact the N-terminal region of the V3-loop backbone (Stanfield *et al.*, 2004). This mode of antigen recognition enables 447-52D to bind a diverse range of V3 sequences. We observe here that a two-residue sequence difference between the UG1033 peptide and the MN peptide previously determined in complex with Fab 447-52D (Arg^{P306}–Ser^{P306} and Ile^{P309}–Leu^{P309}) does not alter the binding interactions between the V3 peptides and Fab. The reported dependence of antigen recognition on the presence of the conserved crown motif GP*x*R (Keller *et al.*, 1993) can be explained in part by the observation that the crown and in particular Arg^{P315} form specific interactions with the antibody-binding site. Finally, the V3-peptide structure shows a high level of structural homology with previously reported V3 crystal and NMR structures, supporting the hypothesis that the V3 loop of gp120 may adopt a conserved structure or limited set of structures, particularly at the crown (Zolla-Pazner, 2004; Ghiara *et al.*, 1994, 1997; Rini *et al.*, 1993; Stanfield *et al.*, 1993, 1999, 2003, 2004; Stanfield, Gorny *et al.*, 2006; Stanfield & Wilson, 2005; Cardozo *et al.*, 2007; Rosen *et al.*, 2006). Future structural studies of such V3-specific neutralizing antibodies in complex with a diverse range of V3 peptides will help to further clarify conserved structural features of the V3 loop, as well as the precise mechanism by which V3 antibodies recognize their epitopes. This information will in turn provide valuable insight into how the V3 region of gp120 may be utilized as an anti-HIV-1 immunogen that may provide some efficacy in combination with immunogens corresponding to other epitopes.

We gratefully acknowledge support by NIH grants GM-46192 (to IAW and RLS), AI36085 (SZP) and HL59725 (SZP), by the NYU Center for AIDS Research (AI27742 to SZP), by the Bill and Melinda Gates Foundation (38631 to SZP), by research funds from the Department of Veterans Affairs (SZP), by the Natural Sciences and Engineering Research Council of Canada (AKD) and by the International AIDS Vaccine Initiative Neutralizing Antibody Consortium (IAW). This is manuscript No. 19279 from The Scripps Research Institute.

References

Back, N. K., Smit, L., De Jong, J. J., Keulen, W., Schutten, M., Goudsmit, J. & Tersmette, M. (1994). *Virology*, **199**, 431–438.
Basmaciogullari, S., Babcock, G. J., Van Ryk, D., Wojtowicz, W. & Sodroski, J. (2002). *J. Virol.* **76**, 10791–10800.
Binley, J. M., Wrin, T., Korber, B., Zwick, M. B., Wang, M., Chappey, C., Stiegler, G., Kunert, R., Zolla-Pazner, S., Katinger, H., Petropoulos, C. J. & Burton, D. R. (2004). *J. Virol.* **78**, 13232–13252.
Brünger, A. T., Adams, P. D., Clore, G. M., DeLano, W. L., Gros, P., Grosse-Kunstleve, R. W., Jiang, J.-S., Kuszewski, J., Nilges, M., Pannu, N. S., Read, R. J., Rice, L. M., Simonson, T. & Warren, G. L. (1998). *Acta Cryst.* D**54**, 905–921.
Burton, D. R., Stanfield, R. L. & Wilson, I. A. (2005). *Proc. Natl Acad. Sci. USA*, **102**, 14943–14948.
Cardozo, T., Kimura, T., Philpott, S., Weiser, B., Burger, H. & Zolla-Pazner, S. (2007). *AIDS Res. Hum. Retroviruses*, **23**, 415–426.
Collaborative Computational Project, Number 4 (1994). *Acta Cryst.* D**50**, 760–763.
Connolly, M. L. (1993). *J. Mol. Graph.* **11**, 139–141.
DeLano, W. L. (2002). *The PyMOL Molecular Graphics System.* http://www.pymol.org.
Gao, F. *et al.* (2005). *J. Virol.* **79**, 1154–1163.
Ghiara, J. B., Ferguson, D. C., Satterthwait, A. C., Dyson, H. J. & Wilson, I. A. (1997). *J. Mol. Biol.* **266**, 31–39.
Ghiara, J. B., Stura, E. A., Stanfield, R. L., Profy, A. T. & Wilson, I. A. (1994). *Science*, **264**, 82–85.
Gorny, M. K., Conley, A. J., Karwowska, S., Buchbinder, A., Xu, J. Y., Emini, E. A., Koenig, S. & Zolla-Pazner, S. (1992). *J. Virol.* **66**, 7538–7542.
Gorny, M. K., Gianakakos, V., Sharpe, S. & Zolla-Pazner, S. (1989). *Proc. Natl Acad. Sci. USA*, **86**, 1624–1628.
Gorny, M. K., Revesz, K., Williams, C., Volsky, B., Louder, M. K., Anyangwe, C. A., Krachmarov, C., Kayman, S. C., Pinter, A., Nadas, A., Nyambi, P. N., Mascola, J. R. & Zolla-Pazner, S. (2004). *J. Virol.* **78**, 2394–2404.
Gorny, M. K., Williams, C., Volsky, B., Revesz, K., Cohen, S., Polonis, V. R., Honnen, W. J., Kayman, S. C., Krachmarov, C., Pinter, A. & Zolla-Pazner, S. (2002). *J. Virol.* **76**, 9035–9045.
Gorny, M. K., Williams, C., Volsky, B., Revesz, K., Wang, X. H., Burda, S., Kimura, T., Konings, F. A., Nadas, A., Anyangwe, C. A., Nyambi, P., Krachmarov, C., Pinter, A. & Zolla-Pazner, S. (2006). *J. Virol.* **80**, 6865–6872.
Gorny, M. K., Xu, J. Y., Gianakakos, V., Karwowska, S., Williams, C., Sheppard, H. W., Hanson, C. V. & Zolla-Pazner, S. (1991). *Proc. Natl Acad. Sci. USA*, **88**, 3238–3242.
Gorny, M. K., Xu, J. Y., Karwowska, S., Buchbinder, A. & Zolla-Pazner, S. (1993). *J. Immunol.* **150**, 635–643.

Goudsmit, J., Debouck, C., Meloen, R. H., Smit, L., Bakker, M., Asher, D. M., Wolff, A. V., Gibbs, C. J. Jr. & Gajdusek, D. C. (1988). *Proc. Natl Acad. Sci. USA*, **85**, 4478–4482.
Hartley, O., Klasse, P. J., Sattentau, Q. J. & Moore, J. P. (2005). *AIDS Res. Hum. Retroviruses*, **21**, 171–189.
Hoffman, T. L. & Doms, R. W. (1999). *Mol. Membr. Biol.* **16**, 57–65.
Huang, C. C., Lam, S. N., Acharya, P., Tang, M., Xiang, S. H., Hussan, S. S., Stanfield, R. L., Robinson, J., Sodroski, J., Wilson, I. A., Wyatt, R., Bewley, C. A. & Kwong, P. D. (2007). *Science*, **317**, 1930–1934.
Huang, C. C., Tang, M., Zhang, M. Y., Majeed, S., Montabana, E., Stanfield, R. L., Dimitrov, D. S., Korber, B., Sodroski, J., Wilson, I. A., Wyatt, R. & Kwong, P. D. (2005). *Science*, **310**, 1025–1028.
Javaherian, K., Langlois, A. J., LaRosa, G. J., Profy, A. T., Bolognesi, D. P., Herlihy, W. C., Putney, S. D. & Matthews, T. J. (1990). *Science*, **250**, 1590–1593.
Javaherian, K., Langlois, A. J., McDanal, C., Ross, K. L., Eckler, L. I., Jellis, C. L., Profy, A. T., Rusche, J. R., Bolognesi, D. P., Putney, S. D. & Matthews, T. J. (1989). *Proc. Natl Acad. Sci. USA*, **86**, 6768–6772.
Jones, T. A. (1982). *FRODO: A Graphics Fitting Program for Macromolecules.* Oxford: Clarendon Press.
Kabat, E. A., Wu, T. T., Reid-Miller, M., Perry, H. M. & Gottesman, K. S. (1987). *Sequences of Proteins of Immunological Interest*, 4th ed. Bethesda: National Institutes of Health.
Keller, P. M., Arnold, B. A., Shaw, A. R., Tolman, R. L., Van Middlesworth, F., Bondy, S., Rusiecki, V. K., Koenig, S., Zolla-Pazner, S., Conard, P., Emini, E. A. & Conley, A. J. (1993). *Virology*, **193**, 709–716.
Koch, M., Pancera, M., Kwong, P. D., Kolchinsky, P., Grundner, C., Wang, L., Hendrickson, W. A., Sodroski, J. & Wyatt, R. (2003). *Virology*, **313**, 387–400.
Krachmarov, C., Pinter, A., Honnen, W. J., Gorny, M. K., Nyambi, P. N., Zolla-Pazner, S. & Kayman, S. C. (2005). *J. Virol.* **79**, 780–790.
Lietzke, S. E., Carperos, V. E. & Kundrot, C. E. (1996). *Acta Cryst.* D**52**, 687–692.
McCaffrey, R. A., Saunders, C., Hensel, M. & Stamatatos, L. (2004). *J. Virol.* **78**, 3279–3295.
McDonald, I. K. & Thornton, J. M. (1994). *J. Mol. Biol.* **238**, 777–793.
Matthews, B. W. (1985). *Methods Enzymol.* **114**, 176–187.
Mbah, H. A., Burda, S., Gorny, M. K., Williams, C., Revesz, K., Zolla-Pazner, S. & Nyambi, P. N. (2001). *J. Virol.* **75**, 7785–7788.
Otwinowski, Z. & Minor, W. (1997). *Methods Enzymol.* **276**, 307–326.
Pantophlet, R., Aguilar-Sino, R. O., Wrin, T., Cavacini, L. A. & Burton, D. R. (2007). *Virology*, **364**, 441–453.
Pantophlet, R. & Burton, D. R. (2006). *Annu. Rev. Immunol.* **24**, 739–769.
Pinter, A., Honnen, W. J., He, Y., Gorny, M. K., Zolla-Pazner, S. & Kayman, S. C. (2004). *J. Virol.* **78**, 5205–5215.
Ratner, L., Fisher, A., Jagodzinski, L. L., Mitsuya, H., Liou, R. S., Gallo, R. C. & Wong-Staal, F. (1987). *AIDS Res. Hum. Retroviruses*, **3**, 57–69.
Richman, D. D., Wrin, T., Little, S. J. & Petropoulos, C. J. (2003). *Proc. Natl Acad Sci. USA*, **100**, 4144–4149.
Rini, J. M., Stanfield, R. L., Stura, E. A., Salinas, P. A., Profy, A. T. & Wilson, I. A. (1993). *Proc. Natl Acad. Sci. USA*, **90**, 6325–6329.
Rizzuto, C. & Sodroski, J. (2000). *AIDS Res. Hum. Retroviruses*, **16**, 741–749.
Rizzuto, C. D., Wyatt, R., Hernandez-Ramos, N., Sun, Y., Kwong, P. D., Hendrickson, W. A. & Sodroski, J. (1998). *Science*, **280**, 1949–1953.
Rosen, O., Chill, J., Sharon, M., Kessler, N., Mester, B., Zolla-Pazner, S. & Anglister, J. (2005). *Biochemistry*, **44**, 7250–7258.
Rosen, O., Samson, A. O., Sharon, M., Zolla-Pazner, S. & Anglister, J. (2006). *Structure*, **14**, 649–651.
Rusche, J. R., Javaherian, K., McDanal, C., Petro, J., Lynn, D. L., Grimaila, R., Langlois, A., Gallo, R. C., Arthur, L. O., Fischinger, P. J., Bolognesi, D. P., Putney, S. D. & Matthews, T. J. (1988). *Proc. Natl Acad. Sci. USA*, **85**, 3198–3202.
Schulze-Gahmen, U., Rini, J. M. & Wilson, I. A. (1993). *J. Mol. Biol.* **234**, 1098–1118.
Sharon, M., Kessler, N., Levy, R., Zolla-Pazner, S., Gorlach, M. & Anglister, J. (2003). *Structure*, **11**, 225–236.
Sharpe, S., Kessler, N., Anglister, J. A., Yau, W. M. & Tycko, R. (2004). *J. Am. Chem. Soc.* **126**, 4979–4990.
Sheriff, S., Hendrickson, W. A. & Smith, J. L. (1987). *J. Mol. Biol.* **197**, 273–296.
Stanfield, R., Cabezas, E., Satterthwait, A., Stura, E., Profy, A. & Wilson, I. (1999). *Structure*, **7**, 131–142.
Stanfield, R. L., Ghiara, J. B., Ollmann Saphire, E., Profy, A. T. & Wilson, I. A. (2003). *Virology*, **315**, 159–173.
Stanfield, R. L., Gorny, M. K., Williams, C., Zolla-Pazner, S. & Wilson, I. A. (2004). *Structure*, **12**, 193–204.
Stanfield, R. L., Gorny, M. K., Zolla-Pazner, S. & Wilson, I. A. (2006). *J. Virol.* **80**, 6093–6105.
Stanfield, R. L., Takimoto-Kamimura, M., Rini, J. M., Profy, A. T. & Wilson, I. A. (1993). *Structure*, **1**, 83–93.
Stanfield, R. L. & Wilson, I. A. (2005). *Hum. Antibodies*, **14**, 73–80.
Stanfield, R. L., Zemla, A., Wilson, I. A. & Rupp, B. (2006). *J. Mol. Biol.* **357**, 1566–1574.
Wei, X., Decker, J. M., Wang, S., Hui, H., Kappes, J. C., Wu, X., Salazar-Gonzalez, J. F., Salazar, M. G., Kilby, J. M., Saag, M. S., Komarova, N. L., Nowak, M. A., Hahn, B. H., Kwong, P. D. & Shaw, G. M. (2003). *Nature (London)*, **422**, 307–312.
Wyatt, R., Kwong, P. D., Desjardins, E., Sweet, R. W., Robinson, J., Hendrickson, W. A. & Sodroski, J. G. (1998). *Nature (London)*, **393**, 705–711.
Zanetti, G., Briggs, J. A., Grunewald, K., Sattentau, Q. J. & Fuller, S. D. (2006). *PLoS Pathog.* **2**, e83.
Zhu, P., Liu, J., Bess, J. Jr, Chertova, E., Lifson, J. D., Grize, H., Ofek, G. A., Taylor, K. A. & Roux, K. H. (2006). *Nature (London)*, **441**, 847–852.
Zolla-Pazner, S. (2004). *Nature Rev. Immunol.* **4**, 199–210.
Zolla-Pazner, S., Zhong, P., Revesz, K., Volsky, B., Williams, C., Nyambi, P. & Gorny, M. K. (2004). *AIDS Res. Hum. Retroviruses*, **20**, 1254–1258.